

# Modeling the Ultrafast Electron Attachment Dynamics of Solvated Uracil

Cate S. Anstöter,<sup>\*,†</sup> Mark DelloStritto,<sup>\*,‡</sup> Michael L. Klein,<sup>\*,‡</sup> and Spiridoula  
Matsika<sup>\*,†</sup>

<sup>†</sup>*Department of Chemistry, Temple University, Philadelphia, PA 19122, USA*

<sup>‡</sup>*Institute for Computational Molecular Science, Temple University SERC, Philadelphia,  
PA 19122, USA*

E-mail: csanstoter@gmail.com; tuh39227@temple.edu; mlklein@temple.edu;  
smatsika@temple.edu

## Abstract

Electron attachment to DNA by low energy electrons can lead to DNA damage, so a fundamental understanding of how electrons interact with the components of nucleic acids in solution is an open challenge. In solution, low energy electrons can generate presolvated electrons,  $e_{pre}^-$ , which are efficiently scavenged by pyrimidine nucleobases to form transient negative ions, able to relax to either stable valence bound anions or undergo dissociative electron detachment or transfer to other parts of DNA/RNA leading to strand breakages. In order to understand the initial electron attachment dynamics, this paper presents a joint molecular dynamics and high-level electronic structure study into the behavior of the electronic states of the solvated uracil anion. Both the valence  $\pi^*$  and non-valence  $e_{pre}^-$  states of the solvated uracil system are studied, and the effect of the solvent environment and the geometric structure of the uracil core are uncoupled to gain insight into the physical origin of the stabilization of the

solvated uracil anion. Solvent reorganization is found to play a dominant role followed by relaxation of the uracil core.

## Introduction

Electron transfer processes in solution phase are ubiquitous in nature, and as such, understanding these intrinsic dynamics is of fundamental importance across a range of interdisciplinary fields. Ionizing radiation processes produce free electrons, the subsequent radiation chemistry of which is determined by the state of solvation of the electrons, their energy, and the electron scavenging ability of neighboring matter.<sup>1</sup> This process is particularly important with regards to DNA damage, as low energy electrons produced by radiation can lead to strand breaks.<sup>2-4</sup> Excess electrons can localize on the nucleobases, leading to a special interest in the electron attachment dynamics of nucleobases over the last decade.

Studies modeling the electron attachment to nucleobases and subsequent reactions, such as dissociative electron attachment, have been carried out previously using high-level *ab initio* methods, predominantly in the gas phase.<sup>5-13</sup> In the gas phase, electron attachment to nucleobases can yield either a fragile dipole bound state or a metastable valence state.<sup>6,14-17</sup> Recently, we used high-level electronic structure methods to elucidate the interplay between electron attachment states of distinctly different characters of bare and mono-hydrated uracil in the gas phase.<sup>17</sup> The two states, the diffuse dipole bound state and the localized valence bound anion, represent the ground anionic state of bare uracil and mono-hydrated uracil, respectively. A series of sophisticated time-resolved photoelectron spectroscopy studies on uracil-water-iodide clusters by the Neumark group probed the changing ultrafast electron attachment dynamics as a function of number of water molecules.<sup>15,18</sup> These studies found that localization of the excess electron to the  $\pi^*$  system of uracil proceeded via the dipole bound state. A recent computational study indicated that dipole bound states cannot persevere past a single solvation shell in solution,<sup>19</sup> therefore electron capture into the  $\pi^*$  system

of solvated uracil must proceed by a different mechanism.

In the condensed phase, it is known that low energy electrons localize rapidly onto nucleobases, forming stable valence bound anions.<sup>20-26</sup> In the solution phase, an important question arises; what is the competition between the solvated electron and the ability of nucleobases to stabilize the excess electron?<sup>27</sup> Pump-probe experiments have provided some valuable insight.<sup>28-30</sup> An elegant experimental study by Ma et al. showed the interplay of the electron scavenger ability of nucleobases with the hydration of electrons in solution.<sup>29</sup> The findings of this study indicated that pyrimidine bases, such as thymine and uracil, are highly efficient electron scavengers able to undergo rapid one electron reduction reactions by the vibrationally excited s-like presolvated electron state,  $e_{pre}^-$ . The initial formation of a transient negative ion rapidly leads to the formation of a stable anion, with no evidence of competition with dissociative electron attachment relaxation pathways. Likewise, molecular dynamics simulations have shown that an excess electron localizes very quickly onto nucleobases, within 5 - 25 fs, such that the water molecules are not able to reorient to form a cavity to solvate the electron.<sup>20,26,31</sup> Moreover, this configuration appears to be the most stable configuration for nucleobase anions, as there is no significant reorientation of the water molecules to create a cavity within roughly 1 ps,<sup>20,26</sup> and calculations of a uracil molecule paired with a solvated electron show rapid electron transfer to uracil.<sup>24,32</sup> In addition, simulations indicate that hydrogen atoms are generally hydrophilic<sup>33</sup> and that solvated electrons in clusters prefer cavities near the cluster surface,<sup>34,35</sup> indicating that solvated electrons would likely migrate quickly to more electronegative sites such as nucleobases. While there have been previous computational efforts to study the uracil anion in solution, these efforts have used relatively small unit cells<sup>20,32,36</sup> without sufficient water molecules to converge the uracil solvation shell or have employed QM/MM methods which are not ideal to yield accurate solvation structures for neutral or anionic uracil.<sup>26</sup> Furthermore, most studies focused on the ground state only, although some recent work has calculated more than one state.<sup>26,36</sup>

Including several electronic states is crucial to understanding the evolution of the elec-

tron attachment dynamics between water and uracil. Furthermore, a toolkit is needed that can capture both the behavior of a nucleobase in water as a bulk property, and the detailed electronic structure of the nucleobase core with high accuracy. The former behavior is best described using molecular dynamics, while the latter requires high-level electronic structure methods. The goal of this work is to employ the best possible approaches for both components in order to have a high quality description of both the bulk solvation and the electronic structure of several electronic states of solvated uracil anion.

In order to study the impact of solvation on the electron attachment dynamics of the uracil anion, we use density functional theory (DFT) based molecular dynamics simulations to generate several independent configurations of the solvated uracil anion. To balance the high computational cost of DFT coupled with a large solvation shell, nine trajectories were generated, allowing adequate sampling of the different solvation structures without the need for longer simulations. This approach also allows us to correlate the electronic structure of the solvated uracil anion with the structure of the solvation shell with a much greater variety of solvation environments than would be available with a single simulation. The electron attachment states to the neutral uracil core were calculated for each independent simulation using equation-of-motion coupled cluster for electron attachment with singles and doubles (EOM-EA-CCSD), which allows for a balanced description of both neutral and several anionic states, combined with effective fragment potential (EFP) which provides a polarizable description of the water environment. This approach allows for an accurate insight into the evolution of the anion, the impact of the solvation structure on the electron localization process, and the ultimate stability of the valence bound anion.

## Methods

Classical molecular dynamics (CMD) simulations of uracil in water were run using the GAFF<sup>37</sup> with the LAMMPS simulation package.<sup>38</sup> Multiple simulations were run with 32,

64, 128, and 256 H<sub>2</sub>O molecules in the NPT ensemble at 330 K, to determine the impact of finite-size effects on the solvation structure of uracil. Note that throughout the simulation procedure an elevated temperature of 330 K was used in order to mimic the impact of nuclear quantum effects. Nuclear quantum effects (NQEs) have a tendency to weaken hydrogen bonds, such that there is a red-shift in the vibrational density of states in the O-H stretching region when including NQEs in a simulation vs using purely classical nuclei. The slightly elevated temperature achieves a similar red-shift in the hydrogen bonds of the system, thereby yielding classical trajectories which more closely match the expected averages yielded from a system with quantum nuclei. This consideration is particularly important for *ab initio* molecular dynamics simulations.<sup>39</sup> Our findings indicate that inclusion of 128 H<sub>2</sub>O molecules was sufficient to converge the radial distribution functions of uracil in water, providing a good balance between cost and accuracy with regards to the *ab initio* simulations. Full results can be found in the Supporting Information (SI).

The initial trajectories were generated using PACKMOL<sup>40</sup> and subsequently equilibrated in the NVT ensemble at 330 K for 1 ns. The system was then equilibrated in the NPT ensemble for 1 ns at the same temperature to confirm the potential was able to accurately reproduce the expected density and to give the system greater freedom to explore possible solvation structures. The unit cell was then deformed over 1 ns to 15.94 Å and then equilibrated the system in the NVT ensemble for a further 1 ns, yielding a density of  $\sim 0.998$  g/cm<sup>3</sup>. To appropriately sample the solvation shell in subsequent DFT simulations, 9 separate and independent simulations with different random initial configurations were run, in order to overcome the issues arising from computationally expensive and thereby short *ab initio* simulations.

Quantum Espresso (v.6.3)<sup>41,42</sup> was used to run Car-Parrinello molecular dynamics simulations<sup>43</sup> of uracil in water. The SCAN functional<sup>44</sup> was used with the HSCV pseudopotentials,<sup>45</sup> a cutoff of 120 Ry, an electron mass of 300 a.u., and a timestep of 4 a.u. while sampling positions every 10 timesteps, yielding a timestep for the atomic trajectories of  $\sim 1$

fs. Using the trajectory equilibrated using CMD, a simulation was run with a lower cutoff of 90.0 Ry for 1 ps at 330 K, to quickly move away from the classical potential energy surface at a lower computational cost. We then ran the *ab initio* simulations of the neutral solvated uracil molecule for 1 ps with a cutoff of 120.0 Ry. Finally, an additional electron was added to the system, the charge was neutralized via a homogeneous positive background. This unit cell was run for a further 1 ps. We studied the final frame of both the neutral uracil simulations and the simulations of the uracil anion. In addition, in order to study the stability of the uracil anion over time using EOM-EA-CCSD, we sampled trajectories of the anion from each simulation every 50 timesteps, corresponding to roughly 48 fs, resulting in 21 snapshots including the final frame.

These structures directly taken from the simulations are the vibrationally hot geometries used for the electronic structure calculations. Additional calculations were done to obtain the neutral and anion equilibrium geometries, in which the hot geometries were optimized using MP2/cc-pVDZ and MP2/aug-cc-pVDZ for the neutral and anion, respectively. Geometries were verified to be minima through vibrational analysis, and the cold geometries were then placed back into the vibrationally hot solvent environment for further electronic structure calculations.

Electronic structure calculations were carried out using the QChem 5.3 computational package.<sup>46</sup> The vertical electron attachment energies were calculated using EOM-EA-CCSD to treat the uracil core, and EFP to treat the 128 water molecules. EFP is a method that can be considered as a sophisticated polarizable model with no fitted parameters, rather all parameters are derived from first principle calculations. This allows accurate representation of the interaction not only between the QM layer and the solvent fragments, but also between the solvent fragments themselves.<sup>47-50</sup> In the QChem implementation of EOM-CC/EFP the solvent response to electron rearrangement in the EOM target states is accounted for using a perturbative non-iterative correction computed for each EOM root.<sup>51,52</sup> The one-electron density of the target excited state is calculated and used to re-polarize the environment.

Specifically, the induced dipoles of the EFP part are recalculated in the field of an excited state, and used to compute the polarization energy corresponding to this state. Preliminary calculations used the Dunning basis set, aug-cc-pVDZ, and further calculations to treat the non-valence presolvated electron states used a aug-cc-pVDZ+3s3p3d basis set. The latter basis set used even-tempered coefficients affixed to a ghost atom placed in the center of the cell, in accordance with previous work.<sup>53</sup>

The size of the basis set required to describe the binding of the presolvated electron state,  $e_{pre}^-$ , was carefully considered. A summary of the findings can be found in the SI. In brief, XsXp and XsXpXd, where X=2-6 shells, were used to calculate the stabilization of the non-valence state. It was found that it was necessary to include Xd shells, but that increasing the number of shells past 3s3p3d lead to negligible difference in the binding energy of the presolvated electron state.

## Results and Discussion

### Simulating Solvated Uracil

The molecular dynamics simulations show that the solvation shell of the uracil molecule depends strongly on both the initial conditions and the charge of the uracil molecule. We note that while the average solvation structure of the neutral uracil molecule closely matches previous *ab initio* simulations,<sup>54</sup> the radial distribution functions (RDFs) of the uracil atoms vary significantly between each simulation. While longer simulations would lead to RDFs which converged to the average, it is clear that more than 1-2 ps is required to yield equilibrium averaged RDFs for the uracil molecule. Therefore, when studying processes such as electron transfer which occur on timescales of 20-100 fs, it is important to generate multiple different configurations in order to understand the impact different solvation structures may have on the result. We find that water molecules form hydrogen-bonds to the oxygen atoms of the neutral uracil molecule with what appears to be a very weak attraction of the hydro-

gen atoms to the carbon atoms (see Figure S4). Upon electron attachment to the valence system of the uracil molecule, we see a contraction of the water-uracil hydrogen bonds and the formation of hydrogen bonds to areas of high  $\pi^*$ -electron density of the uracil anion (see Figure 1). Meanwhile, hydrogen bonds donated from uracil to water molecules are weakened upon electron attachment (Figure S6). These results are consistent with the localization of the excess charge on the uracil molecule, with iterative Hirshfeld charges<sup>55</sup> showing that the charge is localized primarily on the oxygen and carbon atoms of the uracil anion (Table S1).

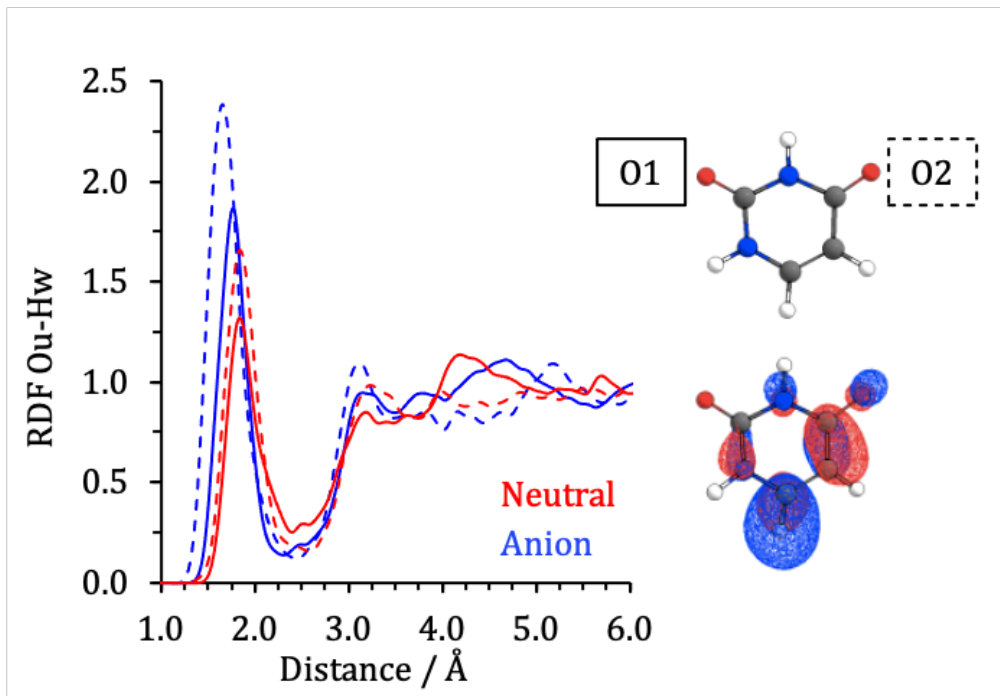


Figure 1: The oxygen uracil to hydrogen water RDFs for the neutral and anion trajectories, plotted individually for the two unique oxygen atoms of the uracil core. Oxygen 1 is shown as solid plots and oxygen 2 as dashed, the sites are identified pictorially to the right of the plots. The representative  $\pi_1^*$  molecular orbital is also shown.

## Time-Dependent Relaxation Dynamics

Having obtained the solvation structure, we move into the examination of the different electronic states that will give information about the evolution of the excess electron. To understand the stabilization of the solvated uracil anion, this paper considers three electron

attachment states (Figure 2). As the attachment energies are calculated relative to the reference neutral state, a positive electron attachment energy denotes a target anionic state that is higher in energy than the neutral ground state, while a negative energy is lower in energy than the neutral ground state. As such, electron attachment to the former leads to formation of a metastable state, while the latter leads to formation of a stable bound anion. This is in contrast to the electron affinity, in which a positive energy denotes a stable bound anion.

Two of the electron attached states considered in Figure 2 are localized valence states, where the excess electron attaches to the  $\pi^*$  system of uracil. The valence states are referred to as the  $\pi_1^*$  and  $\pi_2^*$  states, where the former denotes electron attachment into the LUMO and the latter into the LUMO+1 of neutral uracil. The final state considered is the delocalized non-valence presolvated electron state,  $e_{pre}^-$ . The  $e_{pre}^-$  state considered is the vibrationally hot s-like state. Other delocalized p-like presolvated states with higher energy are also seen in our calculations (see SI), but we are not discussing them further here. We note that the labels s- and p-like refer to the nodal structure of the presolvated electron states, the lowest energy s-like state has no node, while the three p-like states have a single node and differing orientations, analogous to the lowest lying s- and p-atomic orbitals. It is known that electron attachment to the localized valence system of solvated uracil, to form a valence bound anion, proceeds via the non-valence doorway state.<sup>15</sup> In order to capture the correct chemical physics of electron attachment to solvated uracil it is important to include both valence and non-valence states in the model description.

The time dependent stabilization of the valence  $\pi_1^*$  and  $\pi_2^*$  states and non-valence  $e_{pre}^-$  state is estimated using the trajectories from DFT, as shown in Figure 2. For each of the nine trajectories the vertical electron attachment energies were calculated at time steps connecting the equilibrated neutral solvated uracil cell and the equilibrated anionic solvated uracil cell. The rapid relaxation dynamics were calculated with initial time steps of 0, 5, 10, 25, 30 and 50 fs. Slower relaxation dynamics after 50 fs, were calculated at time steps of  $\sim 50$  fs.

Figure 2 shows the averaged vertical electron attachment energies for the three uracil anion states of interest, full details of the results of the individual trajectories can be found in the SI (Figure S9). It should be noted that a proper dynamical study of all these states would require nonadiabatic dynamics including all states, but this is not possible using electronic structure theory that would describe all states correctly.

Notably, the information for the  $\pi_2^*$  and non-valence  $e_{pre}^-$  states should be regarded as qualitative rather than quantitatively correct, when calculated with the aug-cc-pVDZ basis set. This basis set is not sufficient to accurately describe metastable states of anions or non-valence states. However, this basis set is able to accurately describe conventional bound states of anions, such as the  $\pi_1^*$  state. In order to better describe the  $e_{pre}^-$  state a rigid shift was applied to the energies shown in Figure 2. The rigid shift to the non-valence state energies applied was based on the average difference in energy calculated,  $\Delta E = 0.57$  eV, between the electron attachment energies (EAEs) calculated with aug-cc-pVDZ and aug-cc-pVDZ+3s3p3d, using all nine MD neutral  $t=0$  geometries. The uncorrected plot can be found in the SI (Figures S8 and S9).

There are three distinct regions visible in Figure 2. The first is the rapid initial relaxation of the valence states upon addition of the excess electron, highlighted inset, spanning 0 - 50 fs. The next region spans  $\sim 50$  - 275 fs, where a secondary stabilization of the valence states occurs, albeit at a slower pace than the initial response. The final region,  $\sim 250$  - 1000 fs, shows a plateau in the stabilization of all states. The non-valence  $e_{pre}^-$  shows stabilization of the state as the simulation evolves, but this is far less pronounced than for the valence states. The  $\pi_1^*$  state is stabilized by more than 2 eV, the  $\pi_2^*$  state by  $\sim 1.5$  eV and the  $e_{pre}^-$  state by  $\sim 0.4$  eV overall. Figure 2 shows the initial ground state of the uracil anion (lowest energy electron attachment state) at  $t = 0$  to be the  $e_{pre}^-$ , but the rapid stabilization of the  $\pi_1^*$  state leads this becoming the ground state of the anion within  $\sim 15$  fs.

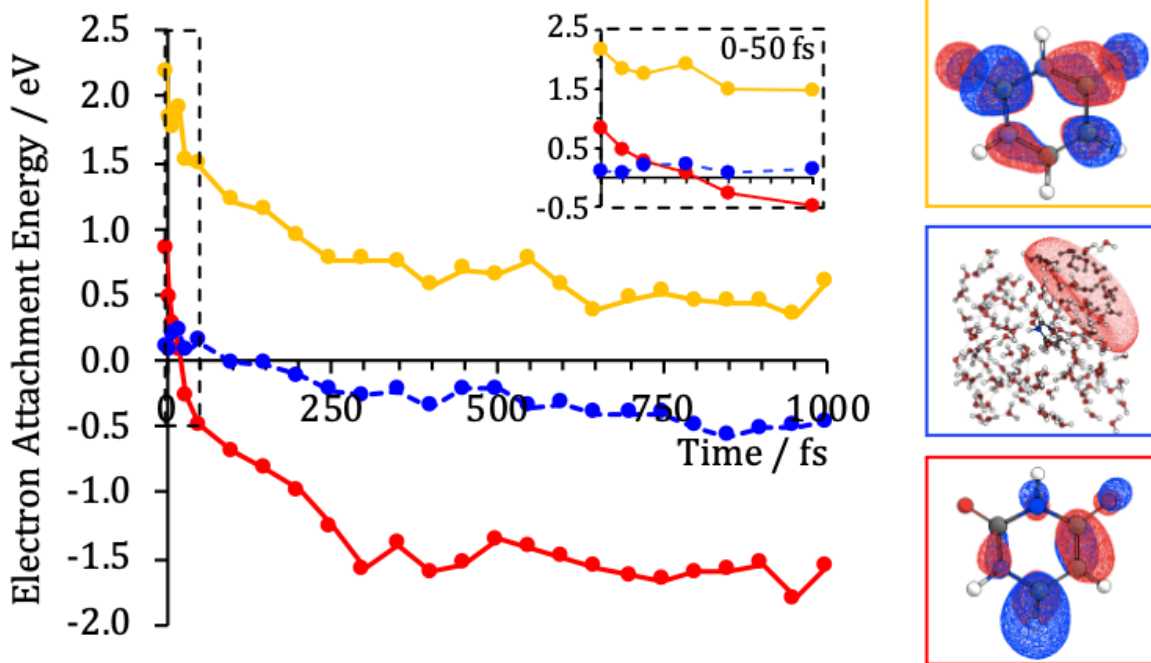


Figure 2: Relative electron attachment energies for the valence and non-valence states of the vibrationally hot uracil core, as a function of simulation time calculated at the EOM-EA-CCSD/aug-cc-pVDZ level.  $t=0$  represents the starting point of an equilibrated neutral solvated uracil cell, and  $t = 1$  ps represents the equilibrated charged solvated uracil cell. At early times, the vertical electron attachment energies were calculated at 0, 5, 10, 25, 30 and 50 fs, to capture the rapid relaxation dynamics of the charged trajectory, amplified and shown inset. After 50 fs, the vertical electron attachment energies were calculated every  $\sim 50$  fs. The energies were calculated for all nine of the MD simulations and averaged. The  $\pi_1^*$ ,  $e_{pre}^-$  and  $\pi_2^*$  states are shown as red, blue and yellow, respectively. A rigid shift of 0.57 eV has been applied to the  $e_{pre}^-$  state energies by comparing the EOM-EA-CCSD/aug-cc-pVDZ with the EOM-EA-CCSD/aug-cc-pVDZ+3s3p3d results. The uncorrected plot can be found in the SI. Representative molecular orbitals denoting these states are shown to the right of the plot, following the same color scheme.

## Geometric and Solvation Effects on Electron Attachment

While Figure 2 gives insight into the stabilization of the valence and non-valence states of the uracil anion, these snapshots are taken directly from the molecular dynamics simulations and as such couple vibrational effects of the uracil core to the rearrangement of the solvent environment. It is desirable to uncouple these two components to gain fundamental insight into the stabilization of the electron attached states.

We first considered the effect of the geometry on the relative energy of the  $\pi_1^*$  state, using the nine equilibrated neutral and anion solvated uracil cells. To uncouple the vibrational effects we reoptimized the uracil core geometry in each of these frames, to the planar minimum energy geometry of the neutral, ( $S_{0eqm}$ ), and the bent minimum energy geometry of the anion, ( $D_{0eqm}$ ). We did this optimization for both neutral trajectories, representing the neutral solvent environment, NT, and for negative ion trajectories, AT, representing the anion solvent environment. The minimum energy geometries were placed back into the solvent environment, and the vertical electron attachment energies were calculated. The results are shown in Figure 3 (a), with representative geometries shown alongside. The averaged energies, for the representative nine trajectories, as a function of solvent and uracil core geometry, are shown in Table 1 for ease of the reader.

Table 1: Vertical attachment energies for the  $\pi_1^*$  and the  $e_{pre}^-$  with respect to both changing geometry of the uracil core and solvent environment. All energies are averages over 9 configurations and are given in eV.

	NT	AT	NT	AT
	$\pi_1^*$	$\pi_1^*$	$e_{pre}^-$	$e_{pre}^-$
$S_{0eqm}$	0.907	-0.572	-	-
$D_{0eqm}$	0.179	-1.691	-	-
$S_{0hot}$	0.837	-	-0.630	-
$D_{0hot}$	-	-1.553	-	-0.640

The equilibrium geometry of the neutral uracil core,  $S_{0eqm}$ , is entirely planar. Electron attachment into the LUMO of the neutral uracil, the  $\pi_1^*$  orbital, causes the uracil core to undergo significant geometric distortion away from the planar equilibrium geometry of the

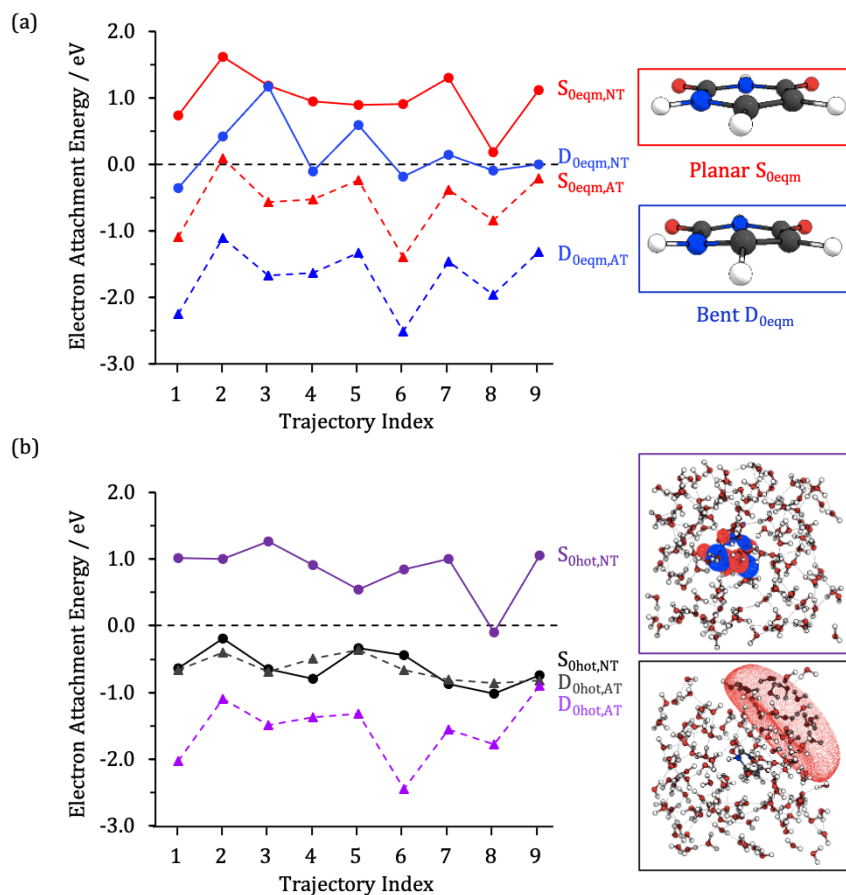


Figure 3: (a) Relative electron attachment energies of the  $\pi_1^*$  state of uracil for nine MD simulations are shown relative to the neutral plus free electron continuum (black dashed line). The energies are shown for the optimized minimum energy geometry of the planar neutral uracil core ( $S_{0eqm}$ , red) and the bent anionic uracil core ( $D_{0eqm}$ , blue), with the solvent structure from the neutral (NT) and charged trajectories (AT). Representative minimum energy geometries are shown to the right. (b) Relative energies of the valence  $\pi_1^*$  (purple) and non-valence  $e_{pre}^-$  (greyscale) for the hot vibrational core of uracil neutral ( $S_{0hot}$ ) and anion ( $D_{0hot}$ ) in the solvent environment of both the neutral and charged trajectories, denoted again as circles and triangles, respectively. Plots depicting the electron density of the respective states are shown to the right, following the same color scheme.

neutral. This distortion leads to a puckering of the ring, due to the anti-bonding nature of the  $\pi_1^*$  orbital across the C-C bonds. In addition, the bonds have different strengths and bond lengths. The C=C and C=O bonds weaken, while the adjacent C-C bond is compressed, as can be predicted by inspection of the nodal structure of the  $\pi_1^*$  orbital (Figure 2). The Cartesian coordinates of the two equilibrium geometries,  $S_{0eqm}$  and  $D_{0eqm}$ , are given in the SI.

The effect of the geometry of the uracil core on the valence  $\pi_1^*$  vertical electron attachment energies can be clearly seen in Figure 3 (a). The bent ( $D_{0eqm}$ ) stabilizes the electron attachment energies relative to the planar ( $S_{0eqm}$ ), by as much as 1 eV, in agreement with previous results investigating the effect of the geometry on the electronic structure for uracil-water clusters in the gas phase.<sup>17</sup> However, the striking effect of the solvent environment can also be clearly observed from both Figure 3 (a) and the averaged values in Table 1. For both the planar and bent geometries calculated in the neutral trajectory solvent environment, NT, the energies tend to lie in the neutral plus free electron continuum. While the bent anion geometry stabilizes the energy relative to the planar geometries, the resultant anionic state is often still metastable or only very loosely bound.

Contrastingly, the electron attached anionic states for snapshots obtained from the anion trajectory solvent environment, AT, tend to be stable bound anions, irrespective of the uracil core geometry, i.e. both  $S_{0eqm,AT}$  and  $D_{0eqm,AT}$  are stable. While both the planar and bent geometries for stable electron attached  $\pi_1^*$  state are bound, it is clear that additional stabilization is afforded in the bent  $D_{0eqm}$  geometry, with the lowest energy (most stable) electron attached states corresponding to that of the  $D_{0eqm,AT}$  from the anion trajectories. The overall stabilization reaches 2.5 eV (see Table 1).

The effect of the solvent environment on both valence and  $e_{pre}^-$  states is considered separately in Figure 3 (b). The vertical electron attachment energies were calculated for both the valence  $\pi_1^*$  state and the non-valence  $e_{pre}^-$  state, using the vibrationally hot uracil core, ( $S_{0hot}$ ) for the neutral and ( $D_{0hot}$ ) for the anion, respectively. The vertical electron attach-

ment energies were calculated using the aug-cc-pVDZ+3s3p3d basis set, in order to be able to accurately treat the very diffuse character of the  $e_{pre}^-$  state. Further details on the justification for the choice of exponents for the 1-electron basis set for the  $e_{pre}^-$  can be found in the SI. Careful treatment of both the valence  $\pi_1^*$  state and the non-valence  $e_{pre}^-$  state allows us to extend analysis of how the reorganization of the solvent environment upon introduction of charge affects these two states of differing character. Inspection of Figure 3 (b) and Table 1 further demonstrates the difference in behavior between the valence and non-valence states upon changing solvent environment. A dramatic lowering in energy of the  $\pi_1^*$  state occurs,  $\Delta E \sim 2.4$  eV, while the energy of the  $e_{pre}^-$  state remains static in energy,  $\Delta E \sim 10$  meV, between the neutral and anion trajectories. A tentative conclusion can be drawn between the relative spatial distribution of the electron density of an electron attached state and the effect of the solvent environment on said electron attached state; the localized electron density of the  $\pi_1^*$  state is far more sensitive to the solvent environment than the highly delocalized  $e_{pre}^-$  state.

To understand and rationalize the reorganization of the solvent environment and the consequential effect on the  $\pi_1^*$  state of the anion we examine the RDFs between the two oxygen atoms of the uracil and the hydrogen atoms of water, Figure 1. This was done for each oxygen atom individually to investigate asymmetry of the solvent environment. The neutral trajectory shows little difference in the RDF of the oxygens, however this become rather pronounced for the anion trajectory. The distance of the anionic O2 RDF is smaller than that of O1, indicating shorter distances between the oxygen atom of the uracil and the hydrogen of the surround water molecules. Comparatively, there is little change between the two oxygen atoms of the neutral trajectory and oxygen 1 of the anion trajectory.

The representative molecule orbital of the  $\pi_1^*$  state, shown inset Figure 1, indicates the cause for the asymmetry in the oxygen RDF. Electron attachment into the  $\pi_1^*$  orbital leads to greater electron density on the O2 atom which, in turn, leads to a greater attraction between the hydrogen bonding pair of oxygen and hydrogen. This interaction between the

anionic uracil core and the solvent environment is crucial in understanding the physical origin of the stabilization of the uracil anion in solution. The role site specific solvation plays in the stabilization of the valence  $\pi_1^*$  state of uracil was previously demonstrated for the monohydrated uracil anion.<sup>17</sup>

From previous work, and indeed within this work, the importance of the formation of explicit hydrogen bonds between water solvent molecules and the heteroatoms of the uracil moiety is shown to be especially important. Specifically, we have consistently found that formation of these bonds between the solvent and the O2 site of uracil leads to an initial stabilization of the valence  $\pi^*$  electron attached state of the anion. Figure 4 provides further information about the nature of bulk solvation, following saturation of heteroatoms with high electron density. This second effect is more subtle, involving tighter solvation around the carbon atoms of the anion, leading to the overall stabilization of the valence bound anion by more than 2 eV. While there may be no true hydrogen-bonds to the central pyridine ring of uracil, we do find that the electrophilic hydrogen atoms of the surrounding water molecules are attracted to the negatively charged carbon atoms of the uracil anion, as evidenced by the RDF from carbon to oxygen of water molecules (see Figure S4). This tighter solvation of the carbons appears to be highly correlated with the EAE of the anion (Figure 4). This is in agreement with previous work on a microsolvated uracil anion<sup>17,21</sup> showing that the valence bound anion is stabilized by the presence of ‘hydrogen-bonds’ to the uracil carbon atoms. Thus, the same stabilization mechanism for the valence bound anion in the microsolvated case also appears in bulk solvation and determines the stability of the solvated anion.

The evolution in the solvation structure over time can also be correlated with the stabilization of the uracil anion observed in Figure 3. A more detailed insight is provided through analysis of the temporal evolution of the RDFs of the oxygen atoms of uracil to the hydrogen atoms of the water molecules, depicted in Figure 5. In particular, Figure 5 reveals the source of the rapid stabilization in the first 50 fs. The hydrogen atoms near the oxygen atoms of uracil reorganize very quickly following the addition of an excess electron, forming

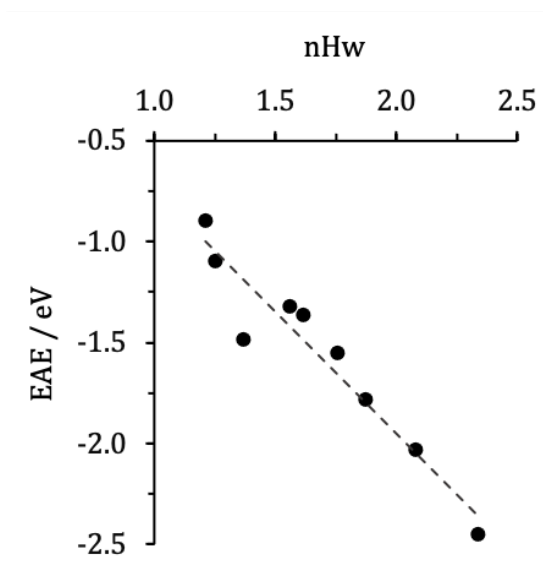


Figure 4: Plot of the correlation between the EAE of the anion and the number of water hydrogen atoms (nHw) in the first solvation shell, determined by integrating the C-Hw RDF up to the first minimum at 3 Å.

new hydrogen-bonds and therefore yielding an increase in the first peak of the RDF within the first 50 fs and then changing little over the rest of the simulation. Detailed information about other changes in the solvation shell can be found in the SI (Figure S11). Specifically, hydrogen-bonds to the  $\pi$ -bound excess electron sites or hydrogen-bonds from uracil to water oxygen atoms tend to equilibrate much more slowly, with major changes in the RDF occurring over 250 - 1000 fs. From this data we can infer that the initial rapid stabilization of the uracil anion is due to the rapid formation of new, stronger hydrogen bonds to uracil oxygen atoms within 50 fs and the stabilization over longer timescales is due to the slower rotation and translation of water molecules as the solvation shell rearranges to the new equilibrium geometry of the anionic uracil core.

Further information on the temporal evolution of the bond lengths of the uracil core geometry, in the identified time regions of importance, provides further insight into what degrees of freedom are evolving in the observed timescales. Full details of all bonds between atoms are given in the SI in Figures S12 and S13. Two bond lengths in particular, the C5-C6 and C4-O8 bonds, give compelling insights into the time scales associated with the uracil core

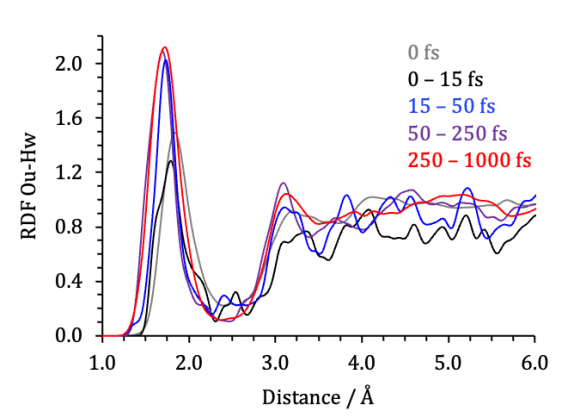


Figure 5: Temporal evolution of the oxygen uracil to hydrogen water RDFs for the distinct relaxation regions linking the neutral and anion trajectories, following the inset color scheme. The neutral is represented by the RDF at 0 fs, while the anion is represented by the RDF 250 - 1000 fs.

relaxation, see Table 2. We note that the time averaged bond lengths are obtained from the SCAN trajectories, while the equilibrium geometries are from MP2 optimisations, for this reason absolute agreement in values at  $t = 0$  and  $t = 1000$  fs is not expected. The equilibrium bond lengths are given for the two critical geometries to demonstrate the expected trend in elongation or contraction as a function of geometric relaxation. Comparison of the trends in relaxation of the C5-C6 and C4-O8 bond lengths with the equilibrium geometries of the neutral and anion, Table 2, indicate that initial relaxation of the hot uracil core occurs on a fairly rapid timescale. For both bonds a rapid change from the neutral core geometry to that representative of the anion core geometry occurs within the first 50 fs. This finding indicates that the relaxation of the core geometry and the response of the hydrogen atoms of water stabilize the formation of the  $\pi_1^*$  state in a concerted fashion, within the initial 0 - 50 fs time region. Other weaker bonds and lower frequency vibrations occur on a slower timescale, between 50-250 fs, providing the additional slower stabilization seen in the 50 - 250 fs time region.

Table 2: Average changes in bond length for the C5-C6 and C4-O8 bonds are given as a function of time regions. All time dependent bond lengths are averages over 9 configurations and are given in Å. The corresponding bond lengths are given for the equilibrium geometries of the planar neutral and bent anion uracil core.

t region / fs	C5-C6 bond length / Å	C4-O8 bond length / Å
0	1.347	1.249
0 - 10	1.378	1.272
10 - 50	1.402	1.303
50 - 250	1.397	1.316
250 - 1000	1.405	1.314
Neutral eqm	1.361	1.223
Anion eqm	1.432	1.262

## The Overall Picture

The results for the time-evolution of the electron attachment states clearly indicate a very rapid localization of the excess electron onto the pyrimidine uracil moiety, via the vibrationally hot  $e_{pre}^-$  state. The electron scavenging occurs very rapidly, within 15 fs, and subsequent stabilization of the localized  $\pi_1^*$  state occurs within the 1 ps simulation time. This two-stage stabilization process is driven by rapid formation of new hydrogen bonds to the uracil oxygen atoms followed by the slower rearrangement of the water molecules within the first solvation shell. This is in agreement with a previous experimental study, in which it was observed that electron irradiation of aqueous uridine monophosphate lead to efficient formation of the electron localizing on the pyrimidine base ring, without any dissociation.<sup>30</sup> The mechanism for the formation of the localized uracil anion was proposed to occur via effective scavenging of the vibrationally hot s-like  $e_{pre}^-$ , as is seen in our study.

The investigation of the effect of the external (solvent) and internal (uracil core geometry) environment on the energetics of the electron attachment states allows us further insight into the physical origin of the stabilization in solution. Using the uncoupled stabilization energies presented in Table 1 we can tentatively apply additional analysis to the different timescales of relaxation dynamics noted in Figure 2. The stabilization of the  $\pi_1^*$  valence state through solvent rearrangement alone (while keeping the uracil geometry frozen) leads

to an energetic stabilization of  $\sim 1.5$  eV or more. There is a far smaller stabilization for the geometric relaxation of the uracil core in the same solvent environment of  $\sim 0.7$  eV. It appears therefore from Figure 2 and Figure 5, that the first rapid stabilization region ( $\sim 1.4$  eV), 0 - 50 fs, must predominantly describe the initial rearrangement of solvent hydrogen bonds from the neutral to anion unit cell. Additional analysis of the changing bond lengths of the uracil core geometry, Table 2, indicates that relaxation of certain bonds also occurs on this rapid timescale. Therefore, the initial rapid stabilization is driven by a concerted response of both the internal and external environment of solvated uracil.

The secondary stabilization is then driven by subsequent concerted mechanism involving the reorientation of the heavier oxygen atoms of water to form hydrogen bonds to areas of high electron density in the  $\pi_1^*$  state and the relaxation of the bonds to nitrogen atoms in the uracil core. The second slower relaxation window, 50 - 275 fs, can be attributed to both the geometric changes of the uracil core and slower relaxations of the solvation shell. The latter region undergoes a stabilization of around  $\sim 1$  eV. We note that our assignment of the primary stabilization being due to the rearrangement of the solvent environment is in agreement with other theoretical studies.<sup>20,32</sup>

The findings of this study indicate the importance of the specific site of solvation, the pattern of explicit hydrogen bonds formed between solvent and anion and the geometry of the uracil core. Previously, the site selective stabilization of monohydrated uracil was investigated, and it was found that solvation of one of the oxygen atoms of uracil lead to formation of a single stable valence bound anion.<sup>17</sup> This oxygen is equivalent to oxygen 2 in Figure 1. Site specific stabilization makes intuitive chemical sense, the electron density of the  $\pi_1^*$  state is localized on the O2 atom, therefore formation of a hydrogen bond between this atom and water stabilizes the excess charge. The ability of additional hydrogen bonds to form at other sites on the uracil leads to further stabilization, but the largest single atom contribution arises from the O2 atom. Additionally, as with the previous study,<sup>17</sup> the vertical electron attachment energy of the valence bound anion of uracil varies dramatically

as a function of the uracil core geometry. As with the gas phase study, electron attachment to the planar geometry of the neutral uracil yields a metastable anion, whereas distortion of the ring toward the bent geometry of the anion leads to a dramatic stabilization in energy. Investigating the effect of the solvent environment and the uracil core geometry allows us to gain insight into how the electron attachment dynamics in the gas phase and solution phase are linked, and therefore we can track the evolution of the electronic structure as a function of the environment.

## Conclusions

We have presented a comprehensive investigation into the physical origin of the electron attachment dynamics of solvated uracil. Through uncoupling the effects of the solvent environment and the uracil core geometry we can rationalize the importance of both components to the overall concerted mechanism that leads to the stabilization of the solvated uracil anion.

We find that initial electron attachment to a neutral solvated uracil unit cell proceeds via the vibrationally hot s-like  $e_{pre}^-$  state, which is the quasi-bound ground state of the anion in this environment. Electron attachment to the  $\pi_1^*$  state yields a metastable state, embedded nearly 1 eV into the neutral plus free electron continuum. Electron attachment causes rapid reorganization to the solvent environment, particularly to the hydrogen bonds to O2 of uracil, within the first  $\sim 50$  fs, particularly pronounced for the valence  $\pi^*$  states. This early stabilization region leads to an inversion of the ground state of the solvated uracil anion within  $\sim 15$  fs. After  $\sim 25$  fs electron attachment to the localized  $\pi_1^*$  state of uracil yields a stable valence bound anion. A secondary relaxation process involving further relaxation of the solvent and of the uracil anion occurs on a longer timescale, whereby the  $\pi^*$  states lower in energy by  $\sim 1$  eV within 250 fs. The geometric and solvent effects are coupled in the investigation of the evolution of electron attachment states over 1 ps. In order to understand the interplay of the individual contributions of the two effects we conducted

additional analysis. We found there to be dramatic differences for the valence and non-valence states. The electron attachment energy of the  $e_{pre}^-$  state shows very little variation as an effect of the solvent environment. However, the  $\pi_1^*$  state shows a total stabilization energy between the final configurations of the neutral and anionic solvent environments of  $\sim 2.4$  eV. The effect of the geometry of the uracil core also plays a large role in the stabilization of the  $\pi_1^*$  state, with the bent anion geometry stabilizing the state by  $\sim 1$  eV compared to the planar neutral geometry.

Using this approach we have determined a lifetime of  $\sim 50$  fs for the localization of the excess electron on uracil, while unravelling the interplay of the stabilization arising from the solvent environment and the geometry of the uracil core. Electron attachment to the neutral uracil core caused the water molecules to rapidly rearrange to form a distinct solvation structure under 50 fs, able to stabilize the valence bound state of the uracil anion. Within this first ultrafast timescale, significant changes to the uracil core geometry also occur, leading to a further stabilization effect. The second, slower stabilization then arises from secondary changes to both the uracil core geometry and the solvent environment. This concerted stabilization yields the formation of the fully solvated valence bound anion within 250 fs. Examination of the final anionic structures, after 1 ps of simulation time, revealed there to be significant variation in the stabilization energy arising from specific solvation configurations. Specifically, the site of solvation through formation of explicit hydrogen bonds between the uracil core and water molecules, plays an important role on the stabilization of the final anionic state. This is in agreement with previous work investigating micro-solvation.<sup>17,21</sup> These results illustrate the importance of properly sampling a full range of possible solvation environments.

We find that electron attachment to uracil in solution proceeds via the diffuse vibrationally hot  $e_{pre}^-$  state, where the excess electron is rapidly scavenged by uracil to form a localized valence bound anion. This finding is in agreement with previous experimental and theoretical studies that concluded that electron attachment to pyrimidinal nucleobases in

water outcompetes the solvation of the free electron, to form  $e_{hyd}^-$  state.<sup>26,29,30,32</sup> The current work provides new insight into how solvent reorganization and internal dynamics in uracil lead to the stabilization and electron dynamics, and highlights the importance of solvent reorganization.

## Acknowledgement

This work was supported by the U.S. Department of Energy, Office of Science, Basic Energy Sciences, under Award No. DE-SC0019394, as part of the Computational Chemical Sciences Program. Calculations were performed using resources of the National Energy Research Scientific Computing Center (NERSC), a U.S. Department of Energy Office of Science User Facility operated under Contract No. DE-AC02-05CH11231.

### Supporting Information:

- Additional RDF plots detailing choice for the number of water molecules and additional solvation structure information.
- The uncorrected electron attachment energies for the  $e_{pre}^-$  state as a function of time.
- Benchmarking data for the basis set choice for the  $e_{pre}^-$  state.
- Cartesian coordinates for the  $S_{0eqm}$  and the  $D_{0eqm}$  minimum energy geometries.

## References

- (1) Kumar, A.; Becker, D.; Adhikary, A.; Sevilla, M. D. Reaction of Electrons with DNA: Radiation Damage to Radiosensitization. *Int. J. Mol. Sci.* **2019**, *20*, 3998.
- (2) Boudaiffa, B.; Cloutier, P.; Hunting, D.; Huels, M. A.; Sanche, L. Resonant Formation of DNA Strand Breaks by Low-Energy (3 to 20 eV) Electrons. *Science* **2000**, *287*, 1658–1660.

- (3) Reisz, J. A.; Bansal, N.; Qian, J.; Zhao, W.; Furdai, C. M. Effects of Ionizing Radiation on Biological Molecules—Mechanisms of Damage and Emerging Methods of Detection. *Antioxid. Redox Signal.* **2014**, *21*, 260–292.
- (4) Alizadeh, E.; Orlando, T. M.; Sanche, L. Biomolecular Damage Induced by Ionizing Radiation: The Direct and Indirect Effects of Low-Energy Electrons on DNA. *Annu. Rev. Phys. Chem.* **2015**, *66*, 379–398.
- (5) Simons, J. How Do Low-Energy (0.12 eV) Electrons Cause DNA-Strand Breaks? *Acc. Chem. Res.* **2006**, *39*, 772–779.
- (6) Sommerfeld, T. Intramolecular Electron Transfer from Dipole-Bound to Valence Orbitals: Uracil and 5-Chlorouracil. *J. Phys. Chem. A.* **2004**, *108*, 9150–9154.
- (7) Sommerfeld, T. Dipole-bound states as doorways in (dissociative) electron attachment. *J. Phys.: Conference Series* **2005**, *4*, 245–250.
- (8) Takayanagi, T.; Asakura, T.; Motegi, H. Theoretical Study on the Mechanism of Low-Energy Dissociative Electron Attachment for Uracil. *J. Phys. Chem. A.* **2009**, *113*, 4795–4801.
- (9) Kumar, A.; Sevilla, M. D. Low-Energy Electron Attachment to 5′-Thymidine Monophosphate: Modeling Single Strand Breaks Through Dissociative Electron Attachment. *J. Phys. Chem. B.* **2007**, *111*, 5464–5474.
- (10) Fennimore, M. A.; Matsika, S. Core-excited and shape resonances of uracil. *Phys. Chem. Chem. Phys.* **2016**, *18*, 30536–30545.
- (11) Fennimore, M. A.; Matsika, S. Electronic Resonances of Nucleobases Using Stabilization Methods. *J. Phys. Chem. A* **2018**, *122*, 4048–4057.
- (12) Fennimore, M. A.; Karsili, T. N. V.; Matsika, S. Mechanisms of H and CO Loss from

- the Uracil Anion Following Low Energy Electron Irradiation. *Phys. Chem. Chem. Phys.* **2017**, *19*, 17233 – 17241.
- (13) Gu, J.; Leszczynski, J.; Schaefer, H. Interactions of electrons with bare and hydrated biomolecules: from nucleic acid bases to DNA segments. *Chem. Rev.* **2012**, *112*, 5603–5640.
- (14) Hendricks, J. H.; Lyapustina, S. A.; de Clercq, H. L.; Bowen, K. H. The dipole bound-to-covalent anion transformation in uracil. *J. Chem. Phys.* **1998**, *108*, 8–11.
- (15) Kunin, A.; Neumark, D. M. Time-resolved radiation chemistry: femtosecond photoelectron spectroscopy of electron attachment and photodissociation dynamics in iodide–nucleobase clusters. *Phys. Chem. Chem. Phys.* **2019**, *21*, 7239–7255.
- (16) Kočišek, J.; Pysanenko, A.; Fárnik, M.; Fedor, J. Microhydration Prevents Fragmentation of Uracil and Thymine by Low-Energy Electrons. *J. Phys. Chem. Lett.* **2016**, *7*, 3401–3405.
- (17) Anstöter, C. S.; Matsika, S. Understanding the Interplay between the Nonvalence and Valence States of the Uracil Anion upon Monohydration. *J. Phys. Chem. A.* **2020**, *124*, 9237–9243.
- (18) Kunin, A.; Li, W.-L.; Neumark, D. M. Dynamics of electron attachment and photodissociation in iodide-uracil-water clusters via time-resolved photoelectron imaging. *J. Chem. Phys.* **2018**, *149*, 084301.
- (19) Anusiewicz, I.; Skurski, P.; Simons, J. Fate of Dipole-Bound Anion States when Hydrated. *J. Phys. Chem. A.* **2020**, *124*, 2064–2076.
- (20) Smyth, M.; Kohanoff, J. Excess Electron Localization in Solvated DNA Bases. *Phys. Rev. Lett.* **2011**, *106*, 238108.

- (21) A. Morgado, C.; Y. Pichugin, K.; Adamowicz, L. Stabilization of an excess electron on uracil by water. *Ab initio* study. *Phys. Chem. Chem. Phys.* **2004**, *6*, 2758–2762.
- (22) Smets, J.; Smith, D. M. A.; Elkadi, Y.; Adamowicz, L. Search for Stable Anions of UracilWater Clusters. Ab Initio Theoretical Studies. *J. Phys. Chem. A.* **1997**, *101*, 9152–9156.
- (23) Dedíková, P.; Neogrady, P.; Urban, M. Electron Affinities of Small UracilWater Complexes: A Comparison of Benchmark CCSD(T) Calculations with DFT. *J. Phys. Chem. A.* **2011**, *115*, 2350–2358.
- (24) Zhao, J.; Wang, M.; Fu, A.; Yang, H.; Bu, Y. Hydrated Electron Transfer to Nucleobases in Aqueous Solutions Revealed by Ab Initio Molecular Dynamics Simulations. *ChemPhysChem* **2015**, *16*, 2348 – 2356.
- (25) McAllister, M.; Smyth, M.; Gu, B.; Tribello, G. A.; Kohanoff, J. Understanding the Interaction between Low-Energy Electrons and DNA Nucleotides in Aqueous Solution. *J. Phys. Chem. Lett.* **2015**, *6*, 3091–3097.
- (26) Mukherjee, M.; Tripathi, D.; Dutta, A. K. Water mediated electron attachment to nucleobases: Surface-bound vs bulk solvated electrons. *J. Chem. Phys.* **2020**, *153*, 044305.
- (27) Alizadeh, E.; Sanche, L. Precursors of Solvated Electrons in Radiobiological Physics and Chemistry. *Chem. Rev.* **2012**, *112*, 5578–5602.
- (28) Wang, C. R.; Nguyen, J.; Lu, Q. B. Bond breaks of nucleotides by dissociative electron transfer of nonequilibrium prehydrated electrons: A new molecular mechanism for reductive DNA damage. *J. Am. Chem. Soc.* **2009**, *131*, 11320–11322.
- (29) Ma, J.; Wang, F.; Denisov, S. A.; Adhikary, A.; Mostafavi, M. Reactivity of prehydrated

- electrons toward nucleobases and nucleotides in aqueous solution. *Science Advances* **2017**, *3*, e1701669.
- (30) Ma, J.; Denisov, S. A.; Marignier, J.-L.; Pernot, P.; Adhikary, A.; Seki, S.; Mostafavi, M. Ultrafast Electron Attachment and Hole Transfer Following Ionizing Radiation of Aqueous Uridine Monophosphate. *J. Phys. Chem. Lett.* **2018**, *9*, 5105.
- (31) Smyth, M.; Kohanoff, J. Excess Electron Interactions with Solvated DNA Nucleotides: Strand Breaks Possible at Room Temperature. *J. Am. Chem. Soc.* **2012**, *134*, 9122–9125.
- (32) Kumar, A.; Adhikary, A.; Shamoun, L.; Sevilla, M. D. Do Solvated Electrons (eaq<sup>-</sup>) Reduce DNA Bases? A Gaussian 4 and Density Functional Theory-Molecular Dynamics Study. *J. Phys. Chem. B* **2016**, *120*, 2115–2123.
- (33) Kim, K. S.; Park, I.; Lee, S.; Cho, K.; Lee, J. Y.; Kim, J.; Joannopoulos, J. D. The Nature of a Wet Electron. *Phys. Rev. Lett.* **1996**, *76*, 956–959.
- (34) Frigato, T.; VandeVondele, J.; Schmidt, B.; Schütte, C.; Jungwirth, P. Ab Initio Molecular Dynamics Simulation of a Medium-Sized Water Cluster Anion: From an Interior to a Surface-Located Excess Electron via a Delocalized State. *J. Phys. Chem. A.* **2008**, *112*, 6125–6133.
- (35) Marsalek, O.; Uhlig, F.; VandeVondele, J.; Jungwirth, P. Structure, Dynamics, and Reactivity of Hydrated Electrons by Ab Initio Molecular Dynamics. *Acc. Chem. Res.* **2012**, *45*, 23–32.
- (36) Cornetta, L. M.; Coutinho, K.; Varella, M. T. d. N. Solvent effects on the  $\pi^*$  shape resonances of uracil. *J. Chem. Phys.* **2020**, *152*, 084301.
- (37) Wang, J.; Wolf, R. M.; Caldwell, J. W.; Kollman, P. A.; Case, D. A. Development and testing of a general amber force field. *J. Comp. Chem.* **2004**, *25*, 1157–1174.

- (38) Plimpton, S. Fast Parallel Algorithms for Short-Range Molecular Dynamics. *J. Comp. Phys.* **1995**, *117*, 1–19.
- (39) Morrone, J. A.; Car, R. Nuclear Quantum Effects in Water. *Phys. Rev. Lett.* **2008**, *101*, 017801.
- (40) Martínez, L.; Andrade, R.; Birgin, E. G.; Martínez, J. M. PACKMOL: A package for building initial configurations for molecular dynamics simulations. *J. Comp. Chem.* **2009**, *30*, 2157–2164.
- (41) Giannozzi, P.; Baroni, S.; Bonini, N.; Calandra, M.; Car, R.; Cavazzoni, C.; Davide Ceresoli,; Chiarotti, G. L.; Cococcioni, M.; Dabo, I.; et al., QUANTUM ESPRESSO: a modular and open-source software project for quantum simulations of materials. *J. Phys. Condens. Matter.* **2009**, *21*, 395502.
- (42) Giannozzi, P.; Andreussi, O.; Brumme, T.; Bunau, O.; Buongiorno Nardelli, M.; Calandra, M.; Car, R.; Cavazzoni, C.; D Ceresoli,; Cococcioni, M.; et al., Advanced capabilities for materials modelling with QUANTUM ESPRESSO. *J. Phys. Condens. Matter* **2017**, *29*, 465901.
- (43) Car, R.; Parrinello, M. Unified Approach for Molecular Dynamics and Density-Functional Theory. *Phys. Rev. Lett.* **1985**, *55*, 2471–2474.
- (44) Sun, J.; Ruzsinszky, A.; Perdew, J. Strongly Constrained and Appropriately Normed Semilocal Density Functional. *Phys. Rev. Lett.* **2015**, *115*, 036402.
- (45) Hamann, D. R.; Schlüter, M.; Chiang, C. Norm-Conserving Pseudopotentials. *Phys. Rev. Lett.* **1979**, *43*, 1494–1497.
- (46) Shao, Y.; Gan, Z.; Epifanovsky, E.; Gilbert, A. T. B.; Wormit, M.; Kussmann, J.; Lange, A. W.; Behn, A.; Deng, J.; Feng, X.; et al., Advances in molecular quantum chemistry contained in the Q-Chem 4 program package. *Mol. Phys.* **2015**, *113*, 184–215.

- (47) Gordon, M. S.; Slipchenko, L. V.; Li, H.; Jensen, J. H. The Effective Fragment Potential: A General Method for Predicting Intermolecular Interactions. *Ann. Rep. Comp. Chem.* **2007**, *3*, 177.
- (48) Gordon, M. S.; Fedorov, D. G.; Pruitt, S. R.; Slipchenko, L. V. Fragmentation Methods: A Route to Accurate Calculations on Large Systems. *Chem. Rev.* **2012**, *112*, 632.
- (49) Gordon, M. S.; Smith, Q. A.; Xu, P.; Slipchenko, L. V. Accurate First Principles Model Potentials for Intermolecular Interactions. *Ann. Rep. Phys. Chem.* **2013**, *64*, 553.
- (50) DeFusco, A.; Minezawa, N.; Slipchenko, L. V.; Zahariev, F.; Gordon, M. S. Modeling Solvent Effects on Electronic Excited States. *J. Phys. Chem. Lett.* **2011**, *2*, 2184–2192.
- (51) Slipchenko, L. V. Solvation of the Excited States of Chromophores in Polarizable Environment: Orbital Relaxation versus Polarization. *J. Phys. Chem. A* **2010**, *114*, 8824–8830.
- (52) Ghosh, D. Hybrid Equation-of-Motion Coupled-Cluster/Effective Fragment Potential Method: A Route toward Understanding Photoprocesses in the Condensed Phase. *J. Phys. Chem. A* **2017**, *121*, 741–752.
- (53) Skurski, P.; Gutowski, M.; Simons, J. How to choose a one-electron basis set to reliably describe a dipole-bound anion. *Int. J. Quantum Chem.* **2000**, *80*, 1024–1038.
- (54) Gageot, M.-P.; Sprik, M. Ab Initio Molecular Dynamics Study of Uracil in Aqueous Solution. *J. Phys. Chem. B.* **2004**, *108*, 7458–7467.
- (55) Bultinck, P.; Van Alsenoy, C.; Ayers, P. W.; Carbó-Dorca, R. Critical analysis and extension of the Hirshfeld atoms in molecules. *J. Chem. Phys.* **2007**, *126*, 144111.

TOC Graphic

